J. Comput. Appl. Res. Mech. Eng. Vol. 11. No. 1, pp. 191-203, 2021 *DOI: 10.22061/JCARME.2020.3973.1469*

SRTTU

Journal of Computational and Applied Research in Mechanical Engineering

jcarme.sru.ac.ir

JCARME

ISSN: 2228-7922

Research paper

Research on the dynamics of a hydraulic static-pile-pressing machine during the process of lifting and slewing of piles

Vinh V. Nguyen, Trung N. Nguyen* and Chi T. Nguyen

Construction Machine Department, University of Transport and Communications, No. 3 Cau Giay Street, Lang Thuong Ward, Dong Da District, Hanoi, Vietnam

Article info:

Article history:

Received: 07/08/2018

Revised: 13/04/2020

Accepted: 07/04/2020

Online: 13/04/2020

Keywords:

Dynamics machine,

Dynamic loading,

Crane,

Hydraulic static-pile-pressing machine.

***Corresponding author:**
nntrung_mxd@utc.edu.vn

Abstract

Information about the dynamic loading of a steel structure is important for its static design as well as for an assessment of its fatigue life. In the case of a hydraulic static-pile-pressing machine, these loads are mainly caused by vibrations and load sway, which occurs as a result of the slewing motion of the boom around the vertical axis and from the radial movement of the load's suspension point. This paper presents the study of the dynamics of a hydraulic static-pile-pressing machine during the process of lifting and slewing a pile using a mounted crane. A six-degree-of-freedom non-linear spatial-dynamic model is employed and a non-linear mathematical model of the machine is formulated. To confirm the mathematical model, the comparison between the measured results and simulation results using the mathematical model shows that the mathematical model is reliable. These results can be used to optimize the machine design based on calculations of its dynamics, fatigue, life expectancy and stability from a dynamic point of view.

1. Introduction

Along with the strong development of the economy, the demand for infrastructures has also increased rapidly: roads, urban areas, industrial parks and commercial centres are being built in ever-increasing numbers. To meet this demand, there has been a rapid development in machinery for foundation work. One machine to which a great deal of attention has been paid is the hydraulic static-pile-pressing machine (hydraulic static-pile driver), which has many outstanding advantages [1]. However, studies of this machine have mainly focused on its work assembly, such as its mechanisms of pile clamping, pile pressing, moving, and the like. The above calculations mainly concern one of a number of specific machine assemblies: calculating and designing the hydraulic system [2–9]; and calculating and designing the detailed steel structure or the details of machine assembly [10–13] from the static point of view. There have

been many studies on the dynamics of construction machines and of cranes, especially boom cranes [14–21]. There are also works that only studied beams on an elastic foundation by Hamilton's principle, but have not studied the whole machine [22–28].

During the process of equipment use, when the crane lifts and slews a pile, the pile will vibrate around the hanging point of the cable at the top of the boom crane with a certain trajectory in space. This oscillation of the pile will create a dynamic force in the cable, the vertical-motion cylinders and the steel structure. It is necessary to study the dynamic parameters (displacement, velocity, acceleration and force) in different working cases of the crane to determine the dynamic coefficient, optimise the design of the steel structure and calculate the fatigue strength and dynamic stability of the machine at work; to which an insufficient amount of attention has been paid by designers.

This paper will present the results of a study on the dynamics of the machine using a six-degree-of-freedom spatial-dynamic model for the typical working cases of the machine: pile lifting, pile slewing, and lifting and slewing at the same time. Details will be presented in the next sections.

2. Pile-lifting and pile-slewing dynamics of the machine

2.1. Introduction to the hydraulic static-pile-pressing machine

Hydraulic static-pile-pressing machines (Fig. 1) are commonly used to press round concrete piles, square piles, H-sections and prefabricated concrete piles with hard foundations in areas where noise and vibration are strictly regulated like around old buildings or in urban areas. The machine is capable of pile up. In addition, this machine is equipped with a hydraulic crane for lifting.

First, the pile is supplied to the piling machine using a crane mounted on the machine, and then, it is inserted into the pressing frame and fixed by the hydraulic cylinders. Then, the pressing cylinders press the piles into the ground. To move, the footsteps of the machine will be controlled and co-ordinated by hydraulic cylinders along the vertical and horizontal footsteps such that the machine can move forwards or backwards or rotate with a small angle [1].

2.2. The study of the dynamics of the machine during simultaneous lifting and slewing of piles

2.2.1. Model description

In Fig. 2, the pile is suspended at a certain height, and the operator will set the lifting mechanism into rewind. The pile will then be lifted, and at the same time, the crane will be slewed to take the pile into the pressing frame.

When the boom crane starts to lift and slew the pile, it should be mounted on the machine, making an initial angle α with the X-axis. The model does not take account of the deformation of the ground, the steel structure of the equipment or the boom of the crane. When the crane is working, because the chassis of the equipment and the counter-weight are very heavy, it is possible to consider the crane slewing mechanism attached to the chassis as fixed (without oscillation). When the lifting mechanism is working, the slewing mechanism of the crane co-operates simultaneously. Other mechanisms of the device (pile clamping, pile driving and moving) are not working.

(a)

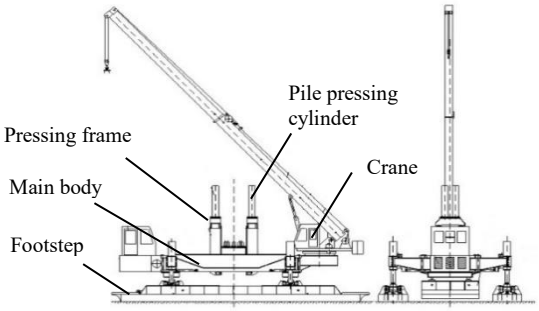

(b)

Fig. 1. A photograph (a) and sketch (b) of a hydraulic static-pile-pressing machine.

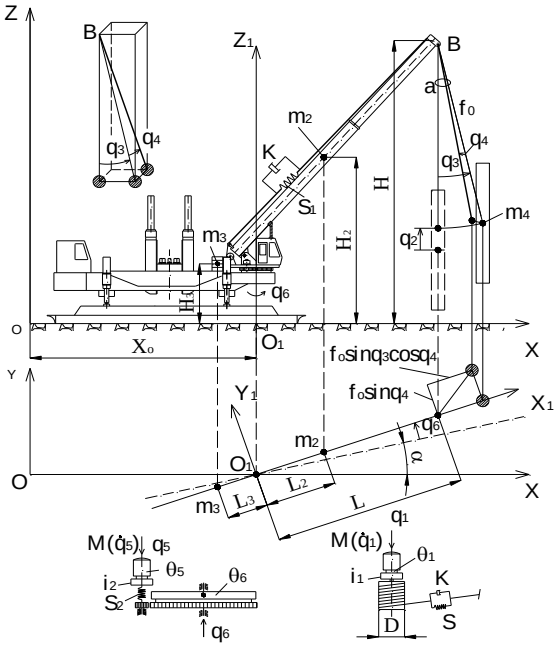

Fig. 2. Model of the dynamics where the machine lifts and slews a pile at the same time.

When the driver starts the engine to slew the crane, the lifting mechanism continues to work, and the suspended pile continues to be lifted with displacement q_2. When the crane is slewing, the pile is considered to be suspended at the top of its boom (point B in Fig. 2). The pile and the crane rope swing in the vertical plane containing the hoist ($X_1O_1Z_1$) at an angle of q_3, swinging in a plane perpendicular to plane ($Y_1O_1Z_1$) at an angle of q_4. The displacement time of the rotation of the hydraulic-slewing motor is represented by q_5, and the rotor has an angular displacement of q_6.

2.2.2. Formulation of the equations of motion

To derive the differential equations of motion, the second-order Lagrange equations of the following form were used:

$$\frac{d}{dt}\left(\frac{\partial T}{\partial \dot{q}_i}\right)-\frac{\partial T}{\partial q_i}+\frac{\partial \Phi}{\partial \dot{q}_i}+\frac{\partial U}{\partial q_i}=Q_i\text{, with i = 1–6.} \tag{1}$$

The positions of point masses m_2, m_3 and m_4 are given by

$$X_2 = X_0 + L_2.cos(q_6 + \alpha) \tag{2}$$
$$Y_2 = L_2.sin(q_6 + \alpha) \tag{3}$$
$$Z_2 = H_2 \tag{4}$$
$$X_3 = X_0–L_3.cos(q_6 + \alpha) \tag{5}$$
$$Y_3 = -L_3.sin(q_6 + \alpha) \tag{6}$$
$$Z_3 = H_3 \tag{7}$$

and

$$X_4 = X_0+(L+f_0.sinq_3.cosq_4).cos(q_6+\alpha) - f_0.sinq_4.sin(q_6+\alpha) \tag{8}$$
$$Y_4 = (L+f_0.sinq_3.cosq_4).sin(q_6+\alpha) + f_0.sinq_4.cos(q_6+\alpha) \tag{9}$$
$$Z_4 = H - f_0.cosq_3.cosq_4 \tag{10}$$

respectively.

The associated speeds are the time derivatives of the positions, and the absolute speeds are the vector sums of the x, y and z components:

$$V_i^2 = \dot{X}_i^2 + \dot{Y}_i^2 + \dot{Z}_i^2\text{ , } i = 2,.,4 \tag{11}$$
$$V_2^2 = \dot{X}_2^2 + \dot{Y}_2^2 + \dot{Z}_2^2 = L_2^2.\dot{q}_6^2 \tag{12}$$
$$V_3^2 = \dot{X}_3^2 + \dot{Y}_3^2 + \dot{Z}_3^2 = L_3^2\dot{q}_6^2 \tag{13}$$
$$\begin{aligned} V_4^2 = {} & \dot{q}_2^2+(f_Q-q_2)^2cos^2q_4.\dot{q}_3^2+(f_Q-q_2)^2.\dot{q}_4^2 \\ & +[L^2+(f_Q-q_2)^2(sin^2q_3cos^2q_4+sin^2q_4) \\ & +2L(f_Q-q_2)sinq_3cosq_4].\dot{q}_6^2 \\ & -2Lsinq_4.\dot{q}_2\dot{q}_6-2(f_Q-q_2)^2cosq_3sinq_4cosq_4.\dot{q}_3\dot{q}_6 \\ & +2(f_Q-q_2)(Lcosq_4+(f_Q-q_2)sinq_3).\dot{q}_4\dot{q}_6 \end{aligned} \tag{14}$$

The kinetic energy of the system is defined as follows. The total kinetic energy, T, must be expressed by means of generalised coordinates. It is the sum of the individual contributions from all mass elements:

$$T=\frac{1}{2}\theta_1\dot{q}_1^2+\frac{1}{2}m_2V_2^2+\frac{1}{2}m_3V_3^2+\frac{1}{2}m_4V_4^2+\frac{1}{2}\theta_5\dot{q}_5^2+\frac{1}{2}\theta_{Z1}\dot{q}_6^2 \tag{15}$$

Substituting values V_2, V_3 and V_4 into the kinetic-energy equation, we have

$$\begin{aligned} T= {} & \frac{1}{2}\theta_1\dot{q}_1^2+\frac{1}{2}m_2L_2^2\dot{q}_6^2+\frac{1}{2}m_3L_3^2\dot{q}_6^2+\frac{1}{2}m_4\{\dot{q}_2^2+(f_Q-q_2)^2cos^2q_4.\dot{q}_3^2 \\ & +(f_Q-q_2)^2.\dot{q}_4^2+[L^2+(f_Q-q_2)^2(sin^2q_3cos^2q_4+sin^2q_4) \\ & +2L(f_Q-q_2)sinq_3cosq_4].\dot{q}_6^2-2Lsinq_4.\dot{q}_2\dot{q}_6 \\ & -2(f_Q-q_2)^2cosq_3sinq_4cosq_4.\dot{q}_3\dot{q}_6 \\ & +2(f_Q-q_2)(Lcosq_4+(f_Q-q_2)sinq_3).\dot{q}_4\dot{q}_6\}+\frac{1}{2}\theta_5\dot{q}_5^2+\frac{1}{2}\theta_{Z1}\dot{q}_6^2 \end{aligned} \tag{16}$$

The dissipation function of the system is given by

$$\Phi = \frac{1}{2}a^2 K\left(R\dot{q}_1 - \dot{q}_2\right)^2 \tag{17}$$

The potential-energy function of the system is the sum of the contributions of the potential terms and is expressed in generalised coordinates as follows:

$$U = \frac{1}{2}S_1\left(\Delta l\right)^2 + \frac{1}{2}S_2\left(\Delta\varphi\right)^2 + m_4 g.Z_4 \tag{18}$$

$$U = \frac{1}{2}S_1\left[\frac{m_4 g}{aS_1} + a\left(Rq_1 - q_2\right)\right]^2 + \frac{1}{2}S_2\left(q_5 - i_2 q_6\right)^2 + m_4 g\left(H - f_0 cosq_3 cosq_4\right) \tag{19}$$

$$\Delta l = \frac{m_4 g}{aS_1} + a\left(Rq_1 - q_2\right) \tag{20}$$

$$f_0 = \left(f_Q - q_2\right) \tag{21}$$

$$\Delta\varphi = \left(q_5 - i_2 q_6\right) \tag{22}$$

The extensive forces are given as

$$\begin{aligned} &Q_1 = M\left(\dot{q}_1\right);\ Q_2 = 0;\ Q_3 = 0; \\ &Q_4 = 0;\ Q_5 = M\left(\dot{q}_1\right);\ Q_6 = M_{cq} \end{aligned} \tag{23}$$

After rearranging the equation, the system of differential equations of motion of the study's mathematical model was derived. This system can be represented in a matrix form as

$$M\ddot{q} + K_1\dot{q}^2 + K_{2i}\dot{q}_2\dot{q}_i + K_{3i}\dot{q}_3\dot{q}_i + K_{6i}\dot{q}_6\dot{q}_i + K_2\dot{q} + Sq = f \tag{24}$$

where the vector components are defined in the Appendix. Eq. (24) represents a system of six second-order non-linear differential equations. This system was solved numerically using the fourth-order Runge–Kutta method. A computer program was developed using MATLAB–Simulink to solve these equations.

2.2.3. Determination of the dynamic force acting on the footsteps (hydraulic cylinders) of the hydraulic static-pile-pressing machine when lifting and slewing piles.

Consider the weight of the machine, which is distributed evenly over the four footsteps:

$$R_j = \frac{G}{4} \pm \frac{M_x}{2b} \mp \frac{M_y}{2a},\ (\text{j} = 1 - 4) \tag{25}$$

$$\text{G} = \text{G}_\text{m} + \text{G}_2 + \text{G}_3 + \text{G}_\text{Q} \tag{26}$$

The momentum on the OX_2-axis is defined as

$$M_x = G_2.L_2.sin(\alpha + q_6) - G_3.L_3.sin(\alpha + q_6) + F_c.L.sin(\alpha + q_6) \tag{27}$$

and that on the OY_2 axis is defined as

$$M_y = G_2[L_{lt} + L_2.cos(\alpha + q_6)] + G_3[L_{lt} - L_3.cos(\alpha + q_6)] + F_c[L_{lt} + L.cos(\alpha + q_6)] \tag{28}$$

Here, G_m is the weight of the machine, G_2 is the weight of the boom crane, G_3 is the weight of the counter-weight, G_Q is the weight of the pile, and F_c is the tension in the cable (Fig. 3).
Therefore, the force applied to each footstep is given by

$$\begin{aligned} &R_1 = \frac{G}{4} + \frac{M_x}{2.b} + \frac{M_y}{2.a};\ R_2 = \frac{G}{4} - \frac{M_x}{2.b} + \frac{M_y}{2.a}; \\ &R_3 = \frac{G}{4} - \frac{M_x}{2.b} - \frac{M_y}{2.a};\ R_4 = \frac{G}{4} + \frac{M_x}{2.b} - \frac{M_y}{2.a} \end{aligned} \tag{29}$$

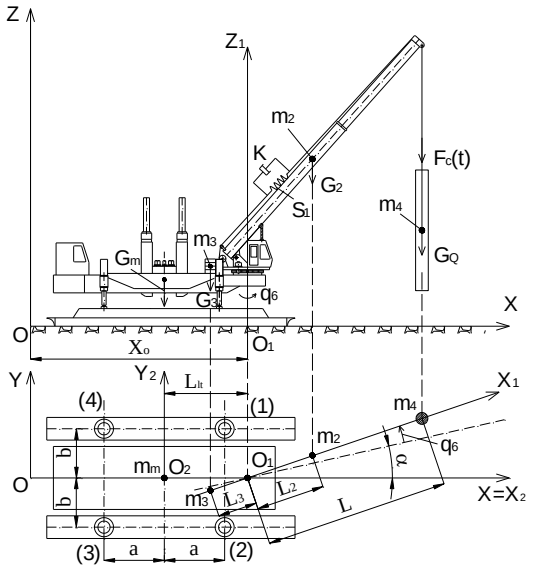

Fig. 3. Model for determining the force acting on the footstep cylinders when the machine lifts and slews a pile at the same time.

When the mathematical model program is used to simulate simultaneous lifting and slewing of a pile followed by braking of the slewing mechanism, we obtain the results given below. The pile is cranked up when the cable (hoist) is stretched while being rotated at the same time. At the 20th second, lifting is halted and slewing commences. By the 30th second, slewing ceases. This program simulates 45 s of movement. After running the computer program, the results presented in Figs. 4-17 are obtained.

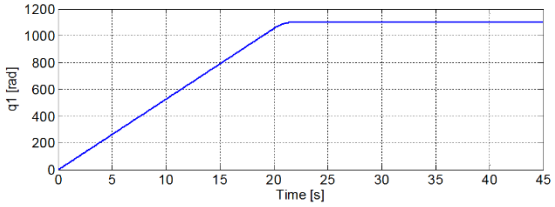

Fig. 4. The angular displacement of the hydraulic motor, q_1 [rad].

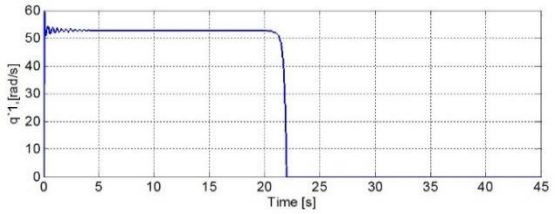

Fig. 5. The rotating speed of the hydraulic motor, $\dot{q}_1$

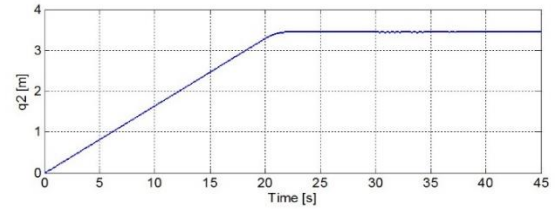

Fig. 6. The displacement of the pile, q_2.

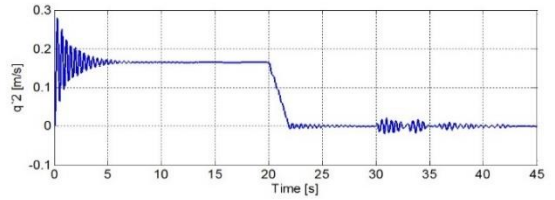

Fig. 7. Velocity of the pile, $\dot{q}_2$

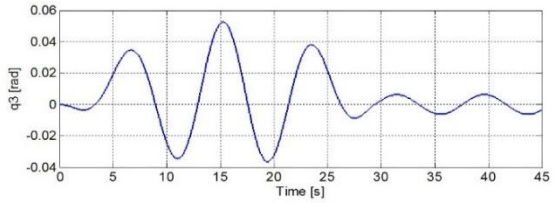

Fig. 8. The shake angle of the pile in the vertical plane containing the hoist ($X_1O_1Z_1$), q_3.

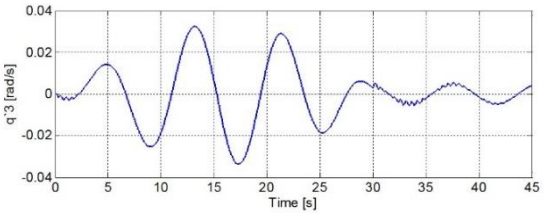

Fig. 9. The angular velocity of the pile in the vertical plane containing the hoist ($X_1O_1Z_1$), $\dot{q}_3$.

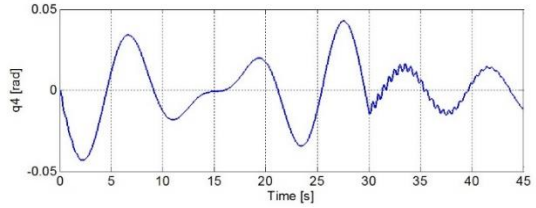

Fig. 10. The shake angle of the pile in the plane perpendicular to that containing the hoist ($Y_1O_1Z_1$), q_4.

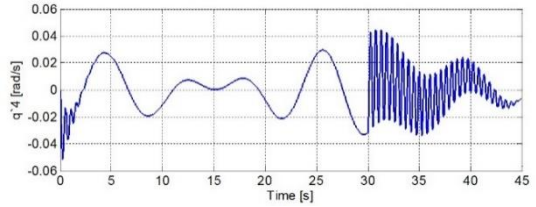

Fig. 11. The angular velocity of the pile in the plane perpendicular to that containing the hoist ($Y_1O_1Z_1$), $\dot{q}_4$.

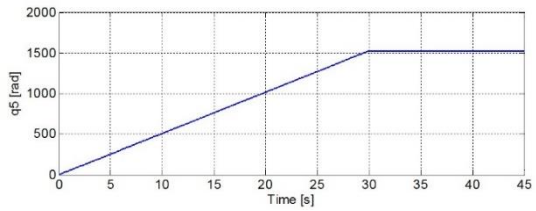

Fig. 12. The angular displacement of the hydraulic motor, q_5.

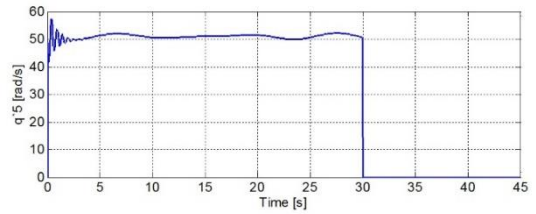

Fig. 13. The rotating speed of the hydraulic motor, $\dot{q}_5$.

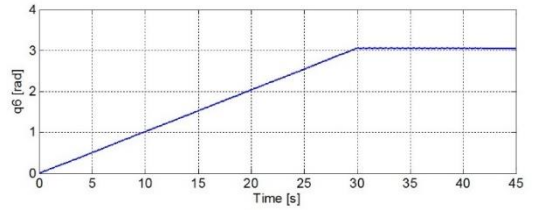

Fig. 14. The angular displacement of the slewing mechanism, q_6.

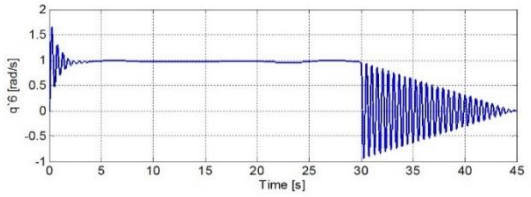

Fig. 15. The rotating speed of the slewing mechanism, $\dot{q}_6$.

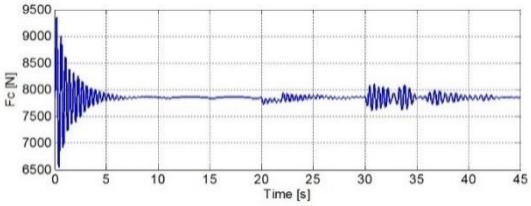

Fig. 16. The dynamic force in the hoist when lifting and slewing the pile.

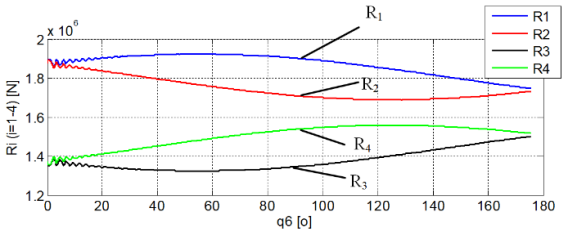

Fig. 17. The forces on the footstep cylinder R_j (j = 1–4) by the rotary angle of the rotor q_6.

Comment:

During the lifting and slewing process, the mathematical model results above show that the dynamic parameters vary greatly at the beginning of the process and then stabilise to their mean values.

Figs. 4 and 5 show that the rotation speed of the hydraulic-lifting motor varies from 0 rad/s to a stabilisation value of 52.6 rad/s in about 4 s. By the 20th second, we start to brake the hydraulic-lifting motor, and its rotation speed tends towards zero.

In Fig. 6, the pile is vertically displaced from 0 to 3.5 m over 20 s. As shown in Fig. 7, the velocity of the pile oscillates for 5 s as the pile begins to lift to a maximum height of 0.279 m/s and then oscillates around the stabilisation value of 0.162 m/s. From 20 s onwards, the pile velocity tends towards 0 m/s.

From Figs. 8 and 9, it can be seen that the shake angle of the pile in the XOZ plane oscillates around the value 0 rad and that the maximum angular-amplitude value is 0.052 rad at 15 s. The angular rotation of the pile in the YOZ plane oscillates around 0 rad, and the maximum angular amplitude is 0.042 rad at 27 s (Figs. 10 and 11).

The rotation speed of the hydraulic-lifting motor oscillates around an average of 51 rad/s, and its maximum value is 57.3 rad/s at 0.4 s (Figs. 12 and 13).

From Figs. 14 and 15, the rotation speed of the slewing mechanism oscillates around an average of 51 rad/s, with a maximum of 57.3 rad/s at 0.4s. The dynamic force in the hoist also varies tremendously in 5 s (Fig. 16), since the pile is lifted up and slewed simultaneously. The maximum dynamic force at the starting time is 9,353 N; then, the value stabilises at 7,848 N.

In Fig. 17, when starting pile lifting and slewing, the values R_1, R_2, R_3, and R_4 fluctuate around their averages. At the start of slewing from 0° to 60°, the R_1 and R_4 values increase, whereas R_2 and R_3 decrease. When slewing from 60° to 120°, the reaction values R_1 and R_2 decrease, whereas R_3 and R_4 increase. When slewing from 120° to 180°, R_1 and R_4 decrease, whereas R_2 and R_3 increase. The variable-force values are shown in Table 1.

3. The measurements

The purpose of these measurements is to determine the dynamic parameters of the hydraulic static-pile-pressing machine in the field. The results of these measurements are used to calculate the dynamics of the machine for comparison with the mathematical model results, and to draw conclusions about the accuracy and reliability of the dynamic model.

Table 1. Forces acting on the footstep cylinders for various slewing angles of the pile.

Forces acting on the footstep cylinders	Angular displacement		
	q_6 (0° to 60°)	q_6 (60° to 120°)	q_6 (120° to 180°)
R_1 (N)	$(1.89–1.92)\times10^6$	$(1.92–1.82)\times10^6$	$(1.82–1.74)\times10^6$
R_2 (N)	$(1.89–1.73)\times10^6$	$(1.73–1.66)\times10^6$	$(1.64–1.74)\times10^6$
R_3 (N)	$(1.35–1.33)\times10^6$	$(1.33–1.40)\times10^6$	$(1.40–1.51)\times10^6$
R_4 (N)	$(1.35–1.49)\times10^6$	$(1.49–1.55)\times10^6$	$(1.55–1.51)\times10^6$

To achieve this goal, the experimental protocol is as follows:

- determine the basic parameters for calculating the dynamics of lifting and slewing piles;
- compare the empirically measured parameters with theoretical calculations to draw conclusions about the validity of the dynamical model.

To achieve the above aims, the experimental measurement should determine the working parameters of the hydraulic static-pile-pressing machine as follows:

- determine the dynamic force in the crane rope during lifting and slewing of the pile;
- determine the dynamic pressure in the footstep cylinders during lifting and slewing of the pile.

The load cell (Bongshin, Korea-DSCK20T) measures the dynamic force in the crane rope and the installation position between the pile and the hook of the crane. The pressure sensor (Huba Control, Switzerland-520.954S) measures the pressure in the footstep cylinders (Figs. 18 and 19). This sensor is attached to the oil pump for the high-pressure chamber of the footstep cylinders.

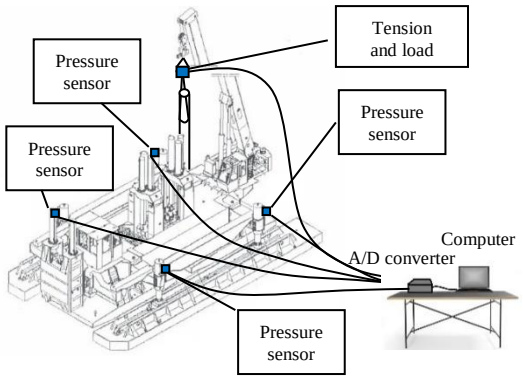

Fig. 18. The layout of the measurement equipment used on the machine when lifting and slewing piles.

4. Comparison of the mathematical model and measurement results

After conducting the measurement, we compared the mathematical model and the experimental results of the dynamic forces in the crane rope in Figs. 20-21.

Fig. 19. The installation position of the load cell and the pressure sensors on the machine.

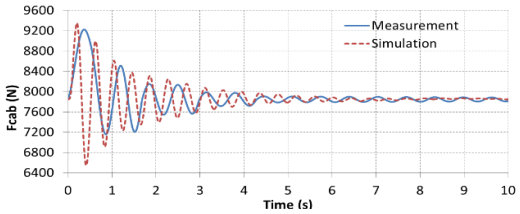

Fig. 20. Dynamic force in the rope when starting to lift and slew the pile simultaneously (from 0 to 10 s).

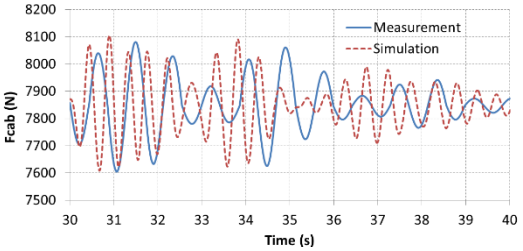

Fig. 21. Dynamic force in the rope when braking the slewing mechanism while slewing the pile (from 30 to 40 s).

Table 2. Dynamic-force coefficients in the process of lifting and slewing a pile.

Working process of machine	Theory			Experiment		
	F_{max} (N)	F_{tb} (N)	k_{si}	F_{max} (N)	F_{tb} (N)	k_{ex}
Starting lifting pile	9354.8	7848.0	1.19	9224.7	7848.6	1.18
Braking slewing pile	8106.0	7848.0	1.03	8080.7	7848.3	1.03

Table 3. Comparison between the mathematical model and measurement deviation in the case of lifting and slewing a pile.

Type of data	Symbol	Starting lifting pile	Braking slewing pile
Theory	$F_{cap}^{max}(N)$	9354.8	8106.0
	$F_{cap}^{tb}(N)$	7848.0	7848.0
	Δ_{lt}	1506.8	258.0
Experiment	$F_{cap}^{max}(N)$	9224.7	8080.7
	$F_{cap}^{tb}(N)$	7848.6	7848.3
	Δ_{tn}	1376.1	232.4
Deviation	$\delta = \frac{\Delta_{lt} - \Delta_{tn}}{\Delta_{lt}} \times 100\%$	8.64%	9.76%

Comment

From Fig. 20 and Table 2, we see that, when the operation of the crane commences, the simulated dynamic force in the crane rope increases for about 0.5 s and then fluctuates around an average value of F_{cab} = 7,848 N. The simulated dynamic coefficient is k_{si} = 1.19. Similarly, in the experiment, the frequency of fluctuation is smaller, but longer and oscillates around the average value F_{cab} = 7,848.6 N. The experimental dynamic coefficient is k_{ex} = 1.18. In terms of shape, the simulated curves are relatively consistent with the experimental ones.

In the progress of braking the slewing mechanism (Fig. 21 and Table 2), the simulated dynamic-force oscillation decreases and then fluctuates around an average value of F_{cab} = 7,848 N; the simulated dynamic coefficient is k_{si} = 1.03. Similarly, in the experimental case, the frequency of fluctuation is smaller but longer, and oscillation occurs around the average value F_{cab} = 7,848.3 N. The experimental dynamic coefficient is k_{ex} = 1.03.

The simulated dynamic coefficient is greater than the experimental dynamic coefficient, and the dynamic coefficient when lifting is larger than that when braking or slewing the pile (Tables 2 and 3).

The mathematical model and measured results of forces on the footsteps of the machine are compared in Figs. 22-25.

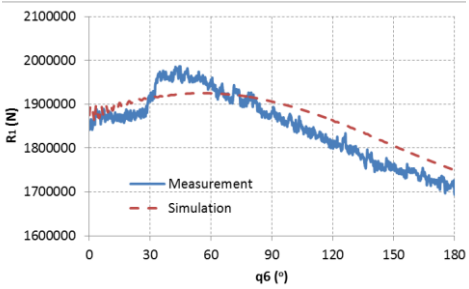

Fig. 22. Force on the 1st footstep cylinder of the machine when lifting and slewing a pile.

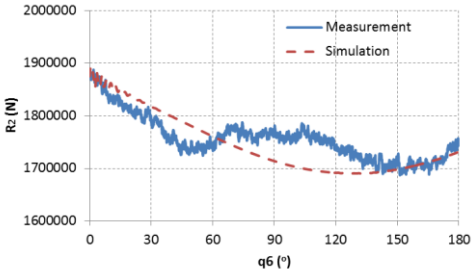

Fig. 23. Force on the 2nd footstep cylinder of the machine when lifting and slewing a pile.

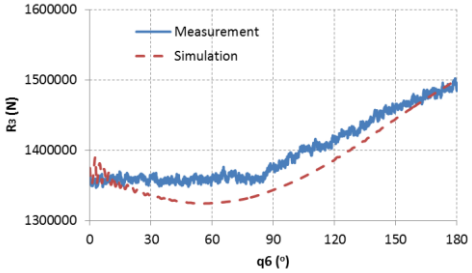

Fig. 24. Force on the 3rd footstep cylinder of the machine when lifting and slewing a pile.

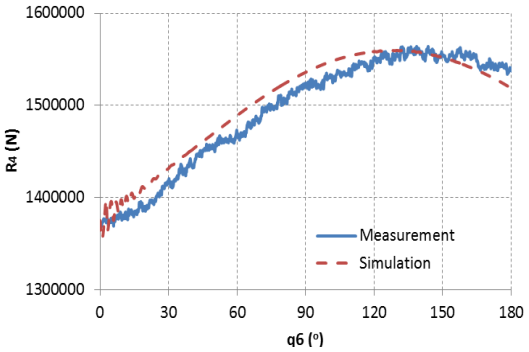

Fig. 25. Force on the 4th footstep cylinders of the machine when lifting and slewing a pile.

Comment

From Figs. 22–25, it can be seen that, when starting the crane and slewing, the values of R_1, R_2, R_3 and R_4 vary depending on the rotational angle of the slewing mechanism. At the start of slewing from 0° to 60°, the reaction-force values R_1 and R_4 will increase, whereas R_2 and R_3 will decrease. When the pile rotates from 60° to 120°, the reaction-force values R_1 and R_2 will decrease, whereas R_3 and R_4 will increase. When turning from 120° to 180°, the reaction-force values R_1 and R_4 will decrease, whereas R_2 and R_3 rise. The changes in these values are shown in the table below (Table 4).

From Figs. 20-25, it can be seen that the graphs of the cable dynamic force and the force acting on the footsteps are the same between the mathematical model and the experiment, confirming the correctness of the model and input value when the calculation is performed according to the theory.

5. Conclusions

In this paper, the mathematical model of the hydraulic static-pile-pressing machine during pile-lifting and pile-slewing motion with five mass elements and six degrees of freedom is presented. Three point masses and two inertial masses are used, enabling a realistic mathematical description of the actual behaviour of the machine. Lagrange equations were used to derive the equations of motion, and a computer program was developed by MATLAB–Simulink to solve these equations. The non-linear mathematical model has no restrictions in term of small angles of the pile sway, making it possible to study the behavior of the machine-mounted crane under real working conditions.

To validate the reliability and correctness of the model, the authors conducted experimental measurements on an actual machine at a construction site. Then, the results of the empirical measurement were compared with those of the mathematical model. The deviation between the two results is in the range of 8–10% because of the assumptions made to simplify the dynamic model.

From the mathematical model, it is possible to survey the factors affecting the mechanical stability of the machine during the process of lifting and slewing of a pile. Our results can be used to calculate and optimise the steel structure of the crane in terms of the fatigue and longevity of the machine.

The mathematical model can be further developed to study the dynamics of other types of hydraulic static-pile-pressing machines.

Table 4. The values of forces on the footstep cylinders for various rotary angles of the pile.

Theorical	0° to 60°	60° to 120°	120° to 180°
R_1 (N)	$(1.89–1.92)\times10^6$	$(1.92–1.82)\times10^6$	$(1.82–1.74)\times10^6$
R_2 (N)	$(1.89–1.73)\times10^6$	$(1.73–1.66)\times10^6$	$(1.64–1.74)\times10^6$
R_3 (N)	$(1.35–1.33)\times10^6$	$(1.33–1.40)\times10^6$	$(1.40–1.51)\times10^6$
R_4 (N)	$(1.35–1.49)\times10^6$	$(1.49–1.55)\times10^6$	$(1.55–1.51)\times10^6$
Measurement	*0° to 60°*	*60° to 120°*	*120° to 180°*
R_1 (N)	$(1.86–1.94)\times10^6$	$(1.94–1.81)\times10^6$	$(1.81–1.72)\times10^6$
R_2 (N)	$(1.88–1.75)\times10^6$	$(1.75–1.73)\times10^6$	$(1.73–1.75)\times10^6$
R_3 (N)	$(1.36–1.37)\times10^6$	$(1.37–1.41)\times10^6$	$(1.41–1.49)\times10^6$
R_4 (N)	$(1.37–1.46)\times10^6$	$(1.46–1.54)\times10^6$	$(1.54–1.55)\times10^6$

6. Acknowledgements

We would like to thank all those people who helped us to prepare this paper. We would like to express our sincere gratitude to Assoc. Prof. Dr. Nguyen Dang Diem, Nguyen Tien Manh engineer, Foundation Engineering and Underground Construction JSC (FECON) and the technical staff of FECON for their supports in the machine measurement process. Their guidance and supports helped us in the time of study and writing of this paper.

Appendix

The ZYJ860B machine is used for measurement and simulation. The input values of the ZYJ860B machine used in Eq. (24) are as follows:

θ_1 = 0,051 kg.m^2; θ_5 = 0,11 kg.m^2; θ_{Z1} = 8 kg.m^2; i_1 = 6,54; i_2 = 500; g = 9,81 m/s^2; a = 6; R = 0,00176; m_2 = 5000 kg; m_3 = 5510 kg; m_4 = 4800 kg; S_1 = 1090581 N/m; S_2 = 50 Nm/rad; K = 2400 Ns/m; f_Q = 12 m; L = 6 m; L_2 = 2,8 m; L_3 = 2 m; $\alpha = 0^o$; $M_{cq} = -(G_d + G_Q).\varpi.sign(\dot{q}_6)$ N.m.

The vector components of Eq. (24) are as follows:

$$M\ddot{q} = \begin{bmatrix} \theta_1 & 0 & 0 & 0 & 0 & 0 \\ 0 & m_4 & 0 & 0 & 0 & -m_4 L.\sin q_4 \\ 0 & 0 & m_4(f_Q-q_2)^2\cos^2 q_4 & 0 & 0 & -m_4(f_Q-q_2)^2\cos q_3 \sin q_4 \cos q_4 \\ 0 & 0 & 0 & m_4(f_Q-q_2)^2 & 0 & m_4(f_Q-q_2).\left((f_Q-q_2)\sin q_3 + L\cos q_4\right) \\ 0 & 0 & 0 & 0 & \theta_5 & 0 \\ 0 & -m_4 L\sin q_4 & -m_4(f_Q-q_2)^2.\cos q_3 \sin q_4 \cos q_4 & m_4(f_Q-q_2)\left((f_Q-q_2)\sin q_3 + L\cos q_4\right) & 0 & \begin{matrix} m_2L_2^2 + m_3L_3^2 + \theta_{Z1} + \\ +m_4.(L+(f_Q-q_2)\sin q_3 \cos q_4)^2 + \\ +m_4(f_Q-q_2)^2\sin^2 q_4 \end{matrix} \end{bmatrix} . \begin{bmatrix} \ddot{q}_1 \\ \ddot{q}_2 \\ \ddot{q}_3 \\ \ddot{q}_4 \\ \ddot{q}_5 \\ \ddot{q}_6 \end{bmatrix} \quad \text{(A.1)}$$

$$K_1\dot{q}^2 = \begin{bmatrix} 0 & 0 & 0 & 0 & 0 & 0 \\ 0 & 0 & m_4(f_Q-q_2)\cos^2 q_4 & m_4(f_Q-q_2) & 0 & m_4\left(L\sin q_3 \cos q_4 + (f_Q-q_2)(\sin q_3^{\,2}\cos q_4^{\,2} + \sin^2 q_4)\right) \\ 0 & 0 & 0 & 0 & 0 & -m_4(f_Q-q_2)(L\cos q_3 \cos q_4 + (f_Q-q_2)\sin q_3 \cos q_3 \cos q_4^{\,2}) \\ 0 & 0 & m_4(f_Q-q_2)^2\sin q_4 \cos q_4 & 0 & 0 & -m_4(f_Q-q_2)\sin q_4.((f_Q-q_2).\cos q_3^{\,2}\cos q_4 - L\sin q_3) \\ 0 & 0 & 0 & 0 & 0 & 0 \\ 0 & 0 & m_4(f_Q-q_2)^2\sin q_3 \sin q_4 \cos q_4 & -m_4(f_Q-q_2)L.\sin q_4 & 0 & 0 \end{bmatrix} . \begin{bmatrix} \dot{q}_1^2 \\ \dot{q}_2^2 \\ \dot{q}_3^2 \\ \dot{q}_4^2 \\ \dot{q}_5^2 \\ \dot{q}_6^2 \end{bmatrix} \quad \text{(A.2)}$$

$$K_{2i}.\dot{q}_2\,\dot{q}_i = \begin{bmatrix} 0 & 0 & 0 & 0 & 0 & 0 \\ 0 & 0 & 0 & 0 & 0 & 0 \\ 0 & 0 & -2m_4(f_Q-q_2).\cos^2 q_4 & 0 & 0 & 0 \\ 0 & 0 & 0 & -2m_4(f_Q-q_2) & 0 & 0 \\ 0 & 0 & 0 & 0 & 0 & 0 \\ 0 & 0 & 2m_4(f_Q-q_2)\cos q_3 \sin q_4 \cos q_4 & -2m_4\left(L\cos q_4 + (f_Q-q_2)\sin q_3\right) & 0 & 0 \end{bmatrix} . \begin{bmatrix} \dot{q}_2\,\dot{q}_1 \\ \dot{q}_2\,\dot{q}_2 \\ \dot{q}_2\,\dot{q}_3 \\ \dot{q}_2\,\dot{q}_4 \\ \dot{q}_2\,\dot{q}_5 \\ \dot{q}_2\,\dot{q}_6 \end{bmatrix} \quad \text{(A.3)}$$

$$K_{3i}\,\dot{q}_3\,\dot{q}_i = \begin{bmatrix} 0 & 0 & 0 & 0 & 0 & 0 \\ 0 & 0 & 0 & 0 & 0 & 0 \\ 0 & 0 & 0 & -2m_4(f_Q-q_2)^2\sin q_4 \cos q_4 & 0 & 0 \\ 0 & 0 & 0 & 0 & 0 & 0 \\ 0 & 0 & 0 & 0 & 0 & 0 \\ 0 & 0 & 0 & 2m_4(f_Q-q_2)^2\cos q_3 \sin q_4^2 & 0 & 0 \end{bmatrix} . \begin{bmatrix} \dot{q}_3\,\dot{q}_1 \\ \dot{q}_3\,\dot{q}_2 \\ \dot{q}_3\,\dot{q}_3 \\ \dot{q}_3\,\dot{q}_4 \\ \dot{q}_3\,\dot{q}_5 \\ \dot{q}_3\,\dot{q}_6 \end{bmatrix} \quad \text{(A.4)}$$

$$K_{6i}\,\dot{q}_6\,\dot{q}_i = \begin{bmatrix} 0 & 0 & 0 & 0 & 0 & 0 \\ 0 & 0 & -2m_4(f_Q-q_2)\cos q_3 \sin q_4 \cos q_4 & 2m_4(f_Q-q_2)\sin q_3 & 0 & 0 \\ 0 & 2m_4(f_Q-q_2)\cos q_3 \sin q_4 \cos q_4 & 0 & -2m_4(f_Q-q_2)^2\cos q_3 \cos^2 q_4 & 0 & 0 \\ 0 & -2m_4(f_Q-q_2)\sin q_3 & 2m_4(f_Q-q_2)^2\cos q_3 \cos^2 q_4 & 0 & 0 & 0 \\ 0 & 0 & 0 & 0 & 0 & 0 \\ 0 & -2m_4\left(\begin{matrix} L\sin q_3 \cos q_4 + \\ +(f_Q-q_2)(\sin q_3^{\,2}\cos q_4^{\,2} + \sin^2 q_4) \end{matrix}\right) & 2m_4(f_Q-q_2)\cos q_3 \cos q_4.\left(L+(f_Q-q_2)\sin q_3 \cos q_4\right) & -2m_4(f_Q-q_2)\sin q_4.\left(\begin{matrix} L\sin q_3 - \\ -(f_Q-q_2)\cos q_3^{\,2}\cos q_4 \end{matrix}\right) & 0 & 0 \end{bmatrix} . \begin{bmatrix} \dot{q}_6\,\dot{q}_1 \\ \dot{q}_6\,\dot{q}_2 \\ \dot{q}_6\,\dot{q}_3 \\ \dot{q}_6\,\dot{q}_4 \\ \dot{q}_6\,\dot{q}_5 \\ \dot{q}_6\,\dot{q}_6 \end{bmatrix} \quad \text{(A.5)}$$

$$K_2\dot{q} = \begin{bmatrix} a^2R^2K & -a^2RK & 0 & 0 & 0 & 0 \\ -a^2RK & a^2K & 0 & 0 & 0 & 0 \\ 0 & 0 & 0 & 0 & 0 & 0 \\ 0 & 0 & 0 & 0 & 0 & 0 \\ 0 & 0 & 0 & 0 & 0 & 0 \\ 0 & 0 & 0 & 0 & 0 & 0 \end{bmatrix} \cdot \begin{bmatrix} \dot{q}_1 \\ \dot{q}_2 \\ \dot{q}_3 \\ \dot{q}_4 \\ \dot{q}_5 \\ \dot{q}_6 \end{bmatrix} \tag{A.6}$$

$$Sq = \begin{bmatrix} a^2R^2S_1 & -a^2RS_1 & 0 & 0 & 0 & 0 \\ -a^2RS_1 & a^2S_1 & 0 & 0 & 0 & 0 \\ 0 & 0 & 0 & 0 & 0 & 0 \\ 0 & 0 & 0 & 0 & 0 & 0 \\ 0 & 0 & 0 & 0 & S_2 & -i_2S_2 \\ 0 & 0 & 0 & 0 & -i_2S_2 & i_2^2S_2 \end{bmatrix} \cdot \begin{bmatrix} q_1 \\ q_2 \\ q_3 \\ q_4 \\ q_5 \\ q_6 \end{bmatrix} \tag{A.8}$$

References

[1] T. N. Nguyen , *Frame design of an 800 tons hydraulic static pile pressing machine with hydraulic footstep type walking mechanism*. Master's thesis, Budapest University of Technology and Economics, Hungary, (2012).

[2] X. Zhou, Q. He, J. Zhu and X. He, "Research on the capacity of hydraulic pile driving under adding force", *2007 Intl. Conf. on Mechatronics Autom., IEEE*, Vol. 4, pp. 2032-2036, (2007).

[3] L. Shou, "The simulation research on hydraulic static pile press machine body leveling movement", *2012 Second Intl. Conf. on Intelligent Syst. Design Eng. Appl., IEEE*, Vol. 2, pp. 1164-1169, (2012).

[4] V. V. Nguyen and T. N. Trung, "Research dynamic of hydraulic transmission system to control pile pressing mechanism of hydraulic pile pressing machine with footstep type walking mechanism", *Proc. Natl. Sci. Technol. Conf. Mech. - Transp. Eng.*, Vol. 5, No. 3, pp. 268-275, (2016).

[5] J. Zhu, Q. He, H. Lin and L. Zhao, "Research and design on multipoint and iso-pressing pile holder mechanism", *J. Constr. Mach.*, Vol. 5, pp. 66-69, (2006).

[6] L. Shuo, "The simulation research and modeling on leveling system of hydraulic static pile driver fuselage", *2013 Fourth Intl. Conf. Digital Manufact. Autom., IEEE*, Vol. 2, pp. 1543-1549, (2013).

[7] J. Hu and X. Lu, "Research on hydraulic control self-levelling system of hydraulic static pile driver", *J. Cent. South Univ.*, Vol. 3, pp.72-74, (2008).

[8] X. Zhou, Q. He, J. Zhu and X. He, "Dynamics modelling and simulation of hydraulic system of pile driving under adding force", *J. Cent. South Univ.*, Vol. 39, No. 2, pp. 322-326, (2008).

[9] X. Zhou, X. Ming, Y. Chen and C. Sun, "Analysis on the strength of pre-fabricated pile under pile clamping", *J. Hunan Univ. of Technol.*, Vol. 24, No. 5, pp. 71-74, (2010).

[10] X. Zhou, Y. Chen and Z. Wang, "Research of the maximum transmission pile driving force of pile clamping mechanism under pile driving", *2011 Intl. Conf. on Mechatronic Sci., Elec. Eng. Comput. (MEC)*, Vol. 3, pp. 2172-2176, (2011).

[11] X. Zhou, R. C. Yu and W. Zhen, "Contact between prefabricated pile and pile clamping jaws under pile driving", *Appl. Mech. Mater.*, Vol. 101-102, pp. 85–91, (2011).

[12] J. Hu, H. Zhu and K. Li, "Stress research and finite element analusis of pile clamping mechanism of hydraulic static pile driver", *Adv. Mater. Res., Switzerland*, Vol. 908, pp. 310-314, (2014).

[13] X. Zhou, Q. Hua and J. Zhu, "Pile clamping mechanism of hydraulic static pile driver based on ANSYS", *J. Cent. South Univ.*, Vol. 40, No. 1, pp. 159-163, (2009).

[14] I. Marinovic, D. Sprecic and B. Jerman, "A slewing crane payload dynamics", *Tehnicki Vjesnik*, Vol. 19, No. 4, pp. 907-912, (2012).
[15] H. Doci, B. Hamidi and S. Lajqi, "Dynamic analysis and control of jib crane in case of jib luffing motion using modelling and simulation", *Int. Fed. Auto. Contr. (IFAC)*, Vol. 49, No. 29, pp. 163-168, (2016).
[16] B. Jerman, P. Podrzaj and J. Kramar, "An investigation of slewing-crane dynamics during slewing motion-development and verification of a mathematical model", *Int. J. Mech. Sci.*, Vol. 46, No. 5, pp. 729-750, (2004).
[17] A. Pristyak and V. V. Nguyen, "Analysis mechanical oscillations and stresses in the mast structure of a Tower crane", *Proceedings of The VIII-th Conf. on Mech. Vibr. T.U. Timisoara, Romania*, Vol. 2, pp. 11-16, (1996).
[18] A. Trabka, "Dynamics of telescopic cranes with flexible structural components", *Int. J. Mech. Sci.*, Vol. 88, pp. 162-174, (2014).
[19] A. Urbas, "Computational implementation of the rigid finite element method in the static and dynamics analysis of forest crane", *Appl. Math. Modell.*, Vol. 46, pp. 750-762, (2016).
[20] H. Lee, "A new design approach for the anti-swing trajectory control of overhead cranes with high-speed hoisting", *Int. J. Control*, Vol. 77, No. 10, pp. 931-940, (2004).
[21] M. P. Cartmell, L. Morrish and A. J. Taylor, "Dynamics of spreader motion in a gantry crane", *Proc. Insitution Mech. Eng., J. Mech. Eng. Sci.*, Vol. 212, No. 2, pp. 85-105, (1998).
[22] A. C. Lynda, B. Fouad, S. Mohamed, Z. Sara, Z. Z. Fatima, T. Abdeldjebbar, D. Abdelhak, A. B. Abdelmoumen and T. Abdelouahed, "Analytical study of bending and free vibration responses of functionally graded beams resting on elastic foundation", *Struct. Eng. Mech.*, Vol. 71, No. 2, pp. 185-196, (2019).
[23] B. Zoulikha, B. Mohammed, B. Fouad, A. B. Abdelmoumen, B. Mohamed, T. Abdelouahed and A. A. Mohammed, "A simple quasi-3D HSDT for the dynamics analysis of FG thick plate on elastic foundation", *Steel Compos. Struct.*, Vol. 31, No. 5, pp. 503-516, (2019).
[24] B. Laid, H. Habib, C. Abdelbaki, A. B. Abdelmoumen, T. Abdelouahed and S. R. Mahmoud, "The effect of parameters of visco-Pasternak foundation on the bending and vibration properties of a thick FG plate", *Geomech. Eng.*, Vol. 18, No. 2, pp. 161-178, (2019).
[25] B. Fouad, A. B. Abdelmoumen, B. Mohamed, A. Abdelghani, Z. Amina and T. Abdelouahed, "Dynamic investigation of porous functionally graded beam using a sinusoidal shear deformation theory", *Wind Struct.*, Vol. 28, No. 1, pp. 19-30, (2019).
[26] B. Boumediene, B. B. Mohamed, B. Fouad, A. B. Abdelmoumen, T. Abdelouahed and S. R. Mahmoud, "Dynamic and bending analysis of carbon nanotube-reinforced composite plates with elastic foundation", *Wind Struct.*, Vol. 27, No 5, pp. 311-324, (2018).
[27] H. Fourn, H. A. Atmane, M. Bourada, A. A. Bousahla, A. Tounsi and S. R. Mahmoud, "A novel four variable refined plate theory for wave propagation in functionally graded material plates", *Steel Compos. Struct.*, Vol. 27, No. 1, pp. 109-122, (2018).
[28] M. Medani, A. Benahmed, M. Zidour, H. Heireche, A. Tounsi, A. A. Bousahla; A. Tounsi and S. R. Mahmoud, "Static and dynamic behavior of (FG-CNT) reinforced porous sandwich plate using energy principle", *Steel Compos. Struct.*, Vol. 32, No. 5, pp. 595-610, (2019).

How to cite this paper:

Vinh V. Nguyen, Trung N. Nguyen and Chi T. Nguyen, "Research on the dynamics of a hydraulic static-pile-pressing machine during the process of lifting and slewing of piles,", *J. Comput. Appl. Res. Mech. Eng.*, Vol. 11, No. 1, pp. 191-203, (2021).

DOI: 10.22061/JCARME.2020.3973.1469

URL: https://jcarme.sru.ac.ir/?_action=showPDF&article=1217